Formation and characterization of neutral krypton and xenon hydrides in low-temperature matrices

Jan Lundell, Leonid Khriachtchev, Mika Pettersson, and Markku Räsänen

Laboratory of Physical Chemistry, University of Helsinki, P. O. Box 55 (A. I. Virtasen aukio 1),
FIN-00014 University of Helsinki, Finland
E-mail: Markku.Rasanen@helsinki.fi

A family of rare-gas containing hydrides HXY (where X = Kr or Xe, Y is an electronegative fragment) is described. These molecules are experimentally prepared in low-temperature matrices by photodissociation of a hydrogen-containing HY precursor and thermal mobilization of the photodetached hydrogen atoms. The neutral HXY molecules are formed in a concerted reaction $H + Y \rightarrow HXY$. Experimental evidence for the formation of these species is essentially based on strong infrared absorption bands that appear after annealing of the photolyzed matrices and are assigned to the X–H stretch of the HXY molecules. Computationally, the formation of these HXY molecules decreases the H–X distance by a factor of ≥ 2 from its van der Waals value, which emphasizes their true chemical bounding possessing both covalent and ionic contributions. The estimated dissociation energies vary from 0.4 to 1.4 eV and keep promises for forthcoming observation of these molecules in the gas phase. The experiments with the HXY molecules widen our knowledge on solid-state photolysis dynamics of hydrogen containing species. In particular, the photolysis of small HY hydrides in solid Xe seems to be a quite local process, and accompanied losses of H atoms play a minor role.

PACS: 82.50. Fv

Introduction

The rare gas atoms have generally been regarded as inert due to their stable electron structure rejecting chemical bond formation capabilities. However, already in 1933 Pauling suggested, based on the consideration of the ionic radii of different elements, that xenon and krypton were capable of forming neutral chemical compounds especially with fluorine [1]. It took three decades before Bartlett was able to make the first rare gas compound [2]. This molecule constituted an ionic $Xe^+[PtF_6]^-$ crystal, which was later shown to consist most probably of a mixture of $XeF^+PtF_6^-$ and $XeF^+Pt_2F_{11}^-$ [3]. Simultaneously with Bartlett's discovery, Hoppe and coworkers were able to isolate XeF_2 [4], and slightly thereafter Claassen et al. prepared XeF_4 [5]. These pioneering findings boosted an enthusiastic research on rare gas containing molecules and several xenon compounds, where Xe was bound to fluorine or oxygen, were reported and reviewed extensively later on [6–16]. The theory of Xe-binding has been authoritatively discussed by Coulson [17].

Neutral xenon-chemistry has been enriched constantly, and several xenon-containing species of similar ionic nature to those of Bartlett's first report have been characterized. The first Xe–N bond was found in $FXeN(SO_2F)_2$ by LeBlond and DesMarteau [18] and many similar but more complex compounds have been characterized since [19–26]. Neutral $FXeCF_3$ and $Xe(CF_3)_2$ have been discussed in the literature [27–29], but neither of them have been spectroscopically characterized. A stable Xe–C bonded molecule, fluorophenylxenon (II) fluoroborate ($[C_6H_5Xe][B(C_6H_5)_3F]$) was reported in 1989 [30] and a number of organoxenonium compounds have been prepared [31,32]. The latest molecule to join the family of organic Xe compounds is $C_6H_5XeF_2^+BF_4^-$ reported in early 2000 by Frohn and coworkers [33]. The chemistry of fluorine-containing rare gas compounds has been recently thoroughly reviewed by Holloway and Hope [34]. Chemistry of krypton is much more sparse than that of Xe. The first Kr-bonds were found in fluorine containing compounds KrF_2 [35–37] and KrF_4 [38] in analogy to xenon. In addition, krypton is known to bind with nitrogen and oxygen, and

these studies have been pioneered by the Schrobilgen group [39–42]. Besides the neutral Xe- and Kr-containing compounds, a large number of ionic rare gas species have been predicted and found, and the reader is encouraged to look, for example, in Refs. 43–47.

The first characterization of KrF_2 and KrF_4 took especially advantage of low-temperature matrix isolation technique, which was originally developed to study unstable molecules and reaction intermediates [48–50]. A studied substance is deposited in large dilution with inert gases on a cold surface or generated photochemically in situ from a precursor molecule already deposited. The solid rare gas environment is regarded as inert towards chemical bond formation and the cage effect is employed to isolate the studied chemical system. Further examples of rare gas containing molecules account, for example, $XeCl_2$ [51], XeClF [37,52] and $FXeBF_2$ [53].

Evidently the formation of such molecules makes the inertness of the solid rare gases questionable and, indeed, recent reviews of photochemical processes in low-temperature matrices underline the interaction between molecular species with the environment upon irradiation [54,55]. These interactions and their consequences on dynamics and chemistry will be discussed in this review, and we will describe solid state synthesis of several HKrY and HXeY (Y = an electronegative fragment) rare-gas containing molecules in low-temperature matrices. It should be emphasized that these molecules are not van der Waals complexes but truly chemically bound species with very characteristic vibrational spectra. The HKrY and HXeY molecules are prepared from a suitable hydrogen-containing precursor (HY), which is photodecomposed producing a hydrogen atom and an electronegative fragment (Y). After preparation of the neutral photoproducts, hydrogen atoms are mobilized thermally. The neutral HKrY and HXeY molecules are then formed in a concerted reaction H + Kr/Xe + Y → → HXeY/HKrY. Quantum chemical calculations are combined with the experimental results to aid the interpretation and understanding of the structure, spectral characteristics, energetics and bonding of these new molecules. The formation of the HKrY and HXeY molecules involves motion of hydrogen atoms and the extent of photo and thermally activated chemical processes highlights the basic concept of fragment mobilization in the solid rare gas lattice. Studies of the formation of HXY molecules at various precursor concentrations and at different extents of photodissociation indicate strongly that the primary photolysis of HY mole-
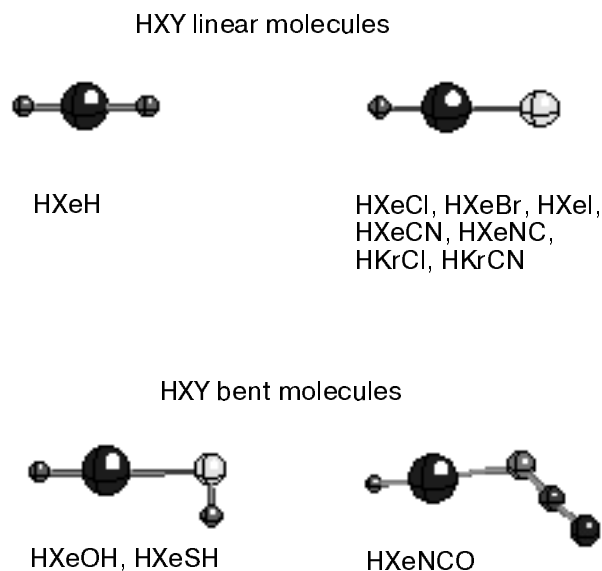
HXY linear molecules

HXeH

HXeCl, HXeBr, HXeI,
HXeCN, HXeNC,
HKrCl, HKrCN

HXY bent molecules

HXeOH, HXeSH   HXeNCO

Fig. 1. The known neutral HKrY and HXeY molecules.

cules is a very local event. We shall show that the analysis involving the novel compounds can shine light to the solid-state dynamics regarding particularly the mobility of H atoms. This review is essentially based on experimental and computational research on the reactivity of rare gases carried mainly out at the Laboratory of Physical Chemistry, University of Helsinki during 1995–1999 [56–69], and all the experimentally observed molecules included in this review are shown in Fig. 1.

Computer experiments on HXeY and HKrY molecules

All the HXY (X = Xe or Kr) molecules have been prepared in solid rare gases and there does not exist experimental data on their geometries and charge distributions. From the computational point of view the rare-gas containing molecules are challenging. The large number of electrons prohibit quite fast the applicability of extensive quantum chemical methods by increasing the computational task beyond the current computer capabilities. As a useful approach, effective core potentials (ECPs) are used, which reduces the number of electrons taken into account in the calculations. Many possible ECPs are available and usually 8 or 18 electrons are included in the valence shell, and the core is substituted by an effective potential resembling the behaviour of the inner electrons. This approach has been taken in all the studies of HXeY and HKrY molecules discussed below, and computational data of the experimentally observed HXeY and HKrY molecules is collected in Table 1.

Table 1

Computational properties of different HXeY and HKrY compounds at the MP2 level [a]

Compound	$r(X-H)$	$r(X-Y)$	r(X-Z)	$q(H)$	$q(X)$	$q(Y)$	$q(Z)$	Dipole moment, D	EA (Y), eV [e]
	Å								
HXeH	1.861			−0.344	0.688			0.0	0.754
HXeSH [b]	1.774	2.729	1.334	−0.226	0.671	−0.435	−0.009	4.5	2.314
HXeI	1.747	3.095		−0.178	0.645	−0.467		6.4	3.059
HXeOH [c]	1.718	2.208	0.962	−0.237	0.818	−0.814	0.232	4.1	1.828
HXeCN	1.707	2.392	1.178	−0.203	0.847	−0.401	−0.242	7.4	3.821
HXeBr	1.694	2.837		−0.156	0.802	−0.647		7.3	3.364
HXeCl	1.685	2.663		−0.165	0.816	−0.651		7.2	3.613
HXeNCO [d]	1.675	2.326	N−C 1.215	−0.169	0.863	−0.566	C 0.263	7.8	
			C−O 1.193				O −0.391		
HXeNC	1.659	2.342	1.187	−0.161	0.880	−0.424	−0.295	9.3	3.821
HKrCN	1.466	2.349	1.177	−0.206	0.886	−0.488	−0.193	9.2	3.821
HKrCl	1.435	2.666		−0.178	0.887	−0.709		9.4	3.613

[a] For Xe and Kr 18-VE ECP and for I 17-VE ECP were used, while all other atoms are described by 6-311++G$(2d,2p)$ basis set. [b] The calculated Xe-S-H angle is 91°. [c] The calculated angles are H−Xe−O 177° and Xe−O−H 109°. [d] The calculated angles H−Xe−N, Xe−N−C and N−C−O are 178°, 125°, and 178°, respectively. [e] Electron affinity, from *Handbook of Chemistry and Physics*, CRC Press, Boca Raton, 72nd ed. (1991).

Calculated structures and energetics. The first computational studies of HXeY and HKrY molecules employed second-order perturbation theory and small basis sets (MP2/LANL1DZ) [53,54]. These calculations are very economic and fast, and at the equilibrium structures they are surprisingly adequate. Up to now our experience of these calculations on the HXeY and HKrY molecules shows that they are able to predict the existence of the molecule. This fact is evidenced for example with halogen containing HKrY molecules. The calculations predict that HKrCl should exist but HKrBr and HKrI are not stable. Indeed, this corresponds to experimental observations and only HKrCl has been isolated in low-temperature matrices [56], but not HKrBr or HKrI despite extensive attempts. These low-level MP2/LANL1DZ calculations give reasonable bond distances and vibrational frequencies. On the other hand, they predict the HXY molecules to be higher in energy than the neutral atomic dissociation limit. For higher level calculations this is reversed as pointed out by Runeberg and cowork-

ers based on their high-level ab initio calculations on HXeH [70,71]. This work is the best and most extensive computation on HXeH, and the authors studied its structural and vibrational properties as well as the energetics at various computational methods from the perturbation theory (MPn) to the state-of-art coupled cluster (CCSD(T)) and multireference configuration interaction (MR-CI) calculations. The study showed that increasing the level of correlation requires also a larger and flexible basis set to achieve chemically reliable results for HXeH. For this molecule, practical methods like MP2 with a standard basis set including multiple polarization and diffuse functions predict a Xe−H bond distance of ca. 1.86 Å. The most extensive CCSD(T) calculations by Runeberg et al. [70,71] estimate the Xe−H bond in HXeH to be ca. 1.95 Å. It must be noted here that this value is much shorter than the Xe−H van der Waals minimum being 3.8 Å [72].

For all known Xe-containing hydrides the MP2 calculations estimate a Xe−H bond between 1.66

and 1.86 Å, the longest Xe–H bond being found for HXeH. It can be noted that the calculated parameters follow a general trend. The H–Xe bond length decreases with the increasing partial positive charge on xenon. The positive charge residing on xenon is largest (+0.88) for the HXeNC molecule corresponding to the shortest Xe–H bond length (1.659 Å). For deeper bound HXeY molecules the contribution of $(HXe)^+$ increases, and the HX bond length approaches the value of the XeH^+ cation, for which computations at the same level predict a bond distance of 1.596 Å. The reason for this is the larger ionic contribution $(HXe)^+Y^-$ in the molecule, and this is discussed in more details below. Similarly for the Kr compounds the increasing charge separation approaches KrH^+ for which the calculated bond distance is 1.382 Å. It is also worth noting that all these molecules have very large dipole moments due to the extensive charge separation.

The HXY molecules observed experimentally up to now are shown in Fig. 1. HXeH is the smallest and simplest of the family of rare gas hydrides but HKrH does not exist neither computationally nor experimentally. One of the hydrogens in these species can be substituted with an electronegative fragment to form a linear HXY molecule, where Y is halogen or a pseudohalogen like CN. A second group of rare-gas containing hydrides is obtained from bent hydrogen containing precursors, and the rare gas atom is inserted into the H–Y bond. Such molecules characterized so far are: HXeOH, HXeSH and HXeNCO. The HXeSH molecule is the first example of a Xe–S bond [60] with a Xe–S–H angle of ca. 91°, which is very similar to the angle of H_2S. Moreover, the calculated S–H bond distance of 1.334 Å is very close to the experimental S–H bond in H_2S being 1.336 Å [73]. Similarly the HXeOH and HXeNCO molecules follow closely the structure of their precursors, i.e., water and HNCO. It appears that the rare gas atom inserted into a covalent H–Y bond has a negligible effect on the rest of the molecule. This observation opens up interesting possibilities that can be in the first place tested by computational methods. The success with Xe insertion into the O–H bond of water prompted us also to test this idea on larger systems. Computations on formic acid indicate that the HCOOXeH molecule is stable, and the HCOO-group is only little perturbed from its structure in the HCOOH monomer [74]. This idea can be extended to other carboxylic acids and amino acids which all behave similarly to formic acid. The largest molecule tested was aspartic acid $(HOOCCH_2CHNH_2COOH)$,

where the most prominent insertion of Xe was noted into the side chain of the molecule. This result suggests that in principle Xe can bind metastably to amino acids, which are building blocks for proteins. In this respect it is important to note that anesthetic substances were suggested to bind directly to proteins, but yet no definitive evidence of the location of the binding sites exists [75]. Since Xe is known to have an anesthetic effect, the insertion of Xe into a covalent O–H bond might have an impact on understanding its anesthetic mechanism.

It should be noted that the HXeY and HKrY molecules are computationally practically linear with respect to the H–Xe–Y bond. For HXeOH the deviation from linearity is about 3° and for the carboxylic and amino acids deviations up to 5° have been reported [74]. For the nitrogen bound Xe compound HXeNCO a few degrees tilt in the H–Xe–N bond is found [68]. Previously also for $FXeOSO_2F$ the F–Xe–O angle was reported to be 177.5° [76], bearing some similarity to the H–Xe–O and H–Xe–N groups in the HXeY molecules. In principle, a simple explanation for this can be found from the three-center four-electron model applied for FXeF [17] and HXeH [70,71]. The highest occupied (σ_g) orbital is centered around the terminal H and F atoms in HXeH and FXeF, respectively. This molecular orbital is nonbonding and occupies two electrons. In HXeH, the lowest orbital (σ_g) is formed from the $5p$ orbital of xenon and the s orbitals of the hydrogens. This molecular orbital possesses additional two electrons and is responsible for the covalent bonding. A similar simple linear model should be valid also for other HXY molecules by replacing the other s orbitals by the proper orbital of the Y fragment. The tilt in the linear bond indicates small external perturbations in the bonding induced by the rest of the molecule.

A model of bonding. Even though the equilibrium structure of the HXeY and HKrY molecules are qualitatively reproduced also with the modest computational approaches compared to the state-of-art approaches, the energetics of the rare-gas containing molecules is more challenging. The origin of the bonding can be understood on the basis of a model where both neutral (HXY) and ionic (HX^+Y^-) bonds contribute. The idea of the ion pair was originally applied on HXe^+Cl^- by Last and George based on semiempirical DIIS calculations [77]. It is informative to discuss the main factors affecting the stability of the HXY molecules. In principle the HXY molecules have strong ionic nature at the equilibrium structure, which is evident from the partial charges in Table 1. This equilibrium structure corresponds to an ion pair disso-

ciation limit $HX^+ + Y^-$. However, when the HXY molecule is stretched along the molecular axis the ionic adiabatic potential surface is crossed by a repulsive surface corresponding to the neutral fragments $H + X + Y$. The dissociation limit of the HXY molecules corresponds to the neutral fragments due to the avoided crossing between the neutral and ionic potential surfaces. Therefore, the ionization potential (IP) of X, electron affinity (EA) of Y and the dissociation energy (D_e) of XH^+ determine the energetics between the neutral and ionic limits. A low ionization potential of X and a large electron affinity of Y are favourable to the formation of HXY. The D_e values of XeH^+ and KrH^+ are about 4.05 and 4.8 eV, respectively [78–81]. The closer the ionic surface lies to the neutral surface, the larger interaction between the two surfaces is expected and the further the avoided crossing is from the HXY minimum. Altogether, there is a rather subtle balance between the different factors affecting the energetics of HXY compounds and their properties depend strongly on Y. One factor is the electron affinity of the Y-fragment (shown in Table 1) and also the effective size of Y. Small Y^- could be thought intuitively to stabilize HXY more than a larger one because it can approach closer to the HX^+ fragment hence producing a larger Coulombic stabilization. This consideration indicates that the lighter rare gases, especially argon, could form similar HArY molecules. However, the ionization potential of Ar is larger (15.759 eV) than that of Kr and Xe, and ArH^+ is less stable (3.87 eV) than KrH^+ and XeH^+ [82]. Nevertheless, based on the simple arguments discussed above argon could combine with an extremely electronegative fragment to form a new HArY molecule. Indeed, computationally both HArCl and HArF have been characterized [56]. CCSD(T)/6-31G(d, p) calculations predict HArF to be the more strongly bound of these two molecules with a binding energy of 0.2 eV [56].

In terms of resonance structures, HXY should be described as a resonance hybrid between several possible structures, the most important being HX^+Y^-. The other important structures are neutral $H-X-Y$ and ionic H^-X^+Y. The ionic structures tend to stabilize the compound and the neutral structure destabilizes it. Recently, the bonding nature of HXY molecules has been studied by topological analysis of the Electron Localization Function (ELF), in which three different resonance structures were considered: H^+XY^-, HX^+Y^- and HX^-Y^+ [83]. For HXeCl and HKrCl the second structure has the largest weight being about 60%. For the first structure the approximate weight is about 20%, and the remaining 20% resides on the structure with the positive charge localized on the halogen. Therefore, it was concluded that the positive charge is mainly localized on the rare gas atom, and that the H–X bond was mostly covalent in nature. It was concluded about the interaction between the rare gas atom and the halogen that this binding is mostly of a so called unshared-electron type, i.e., the interaction is mainly ionic but with a nonnegligible fraction of a covalent character. This conclusion is in agreement with the simple model derived above where both neutral and ionic potential surfaces contribute to the HXY molecule.

The H–X bond distance reflects directly the fraction of the ionic contribution in the molecule. The computationally strongest HXY molecule among the experimental observed ones is HXeCN, which has a dissociation energy of 1.43 eV [59] with respect to the dissociation limit $H + Xe + CN$. CISD (configuration interaction with single and double excitations) calculations on HXeCl estimate the binding energy to be 0.9 eV, and also the first excited state was found to include a minimum in accordance with the curve crossing. The first excited state was calculated to be bound by 2.0 eV and lie almost 5 eV above the ground state at the $X^1\Sigma^+$ equilibrium structure [84]. In general, computationally the ground state HXY molecules are bound by 0.4–1.4 eV.

Vibrational properties. The agreement of the calculated and experimental vibrational frequencies reflect the adequacy of the potential energy surface by a given theoretical approach. As noted above, the equilibrium structures are reasonably well reproduced already at modest computational levels, and therefore the vibrational frequencies are also qualitatively correct. However, the HXY molecules are relatively weakly bound and the potential energy surface near the dissociation limit can not be described accurately without extensive basis sets and electron correlation. For HXeH the MP2 calculation gives the following frequencies: symmetric stretch at 1559 cm^{-1}, antisymmetric stretch at 1385 cm^{-1} and bending at 876 cm^{-1}. Increasing the electron correlation to CCSD(T) decreases both the symmetric and the antisymmetric stretches to 1279 and 1216 cm^{-1}, respectively [70,71]. Also, the CCSD(T) calculations predict the bending mode at 773 cm^{-1}. Recently we studied the effect of anharmonicity for HXeH at the MP2 level, and found that both the antisymmetric stretch and the bending modes are much more harmonic than the symmetric stretch [85]. These results are collected in Table 2 and compared with the harmonic MP2 and CCSD(T) results. The symmetric stretch, which

Table 2

Comparison of calculated and measured vibrational frequencies of some HXeY compounds. The numbers in the parentheses are the IR intensities[a] (in $km \cdot mol^{-1}$)

Compound	ν (Xe–H)	2ν (Xe–H)	δ (H–Xe–Y)	2δ (H–Xe–Y)	ν (Xe–Y)
HXeH					
MP2 harm.	1385 (2503)		876 (69)		1559 (0)
CCSD(T) harm.	1279		773	1666 (0)	1216
MP2 anharm.	1337 (4594)	2648 (0)	839 (69)		1469 (0)
Experiment	1166, 1181		701		840 [b]
HXeCl					
MP2 harm.	1740 (2058)		595 (4)		267 (46)
MP2 anharm.	1642 (1288)	3194 (20)	577 (2)	1143 (0)	260 (2)
Experiment	1648				
HXeBr					
MP2 harm.	1679 (4102)		526 (1)		182 (29)
MP2 anharm.	1544 (1445)	2967 (15)	506 (2)	997 (33)	180 (48)
Experiment	1504	2869	489	965	
HXeI					
MP2 harm.	1514 (5423)		500 (1)		143 (18)
MP2 anharm.	1359 (2429)	2585 (51)	477 (1)	937 (44)	142 (38)
Experiment	1193	2190	450	886, 896	129 [c]
HXeOH					
MP2 harm.	1823 (1456)		653 (7) [d]		437 (126) [e]
CCSD(T) harm.	1678		629 [d]		419 [e]
MP2 anharm.	1713 (1043)	3342 (12)	627 (5) [d]	1242 (4)	425 (269) [e]
Experiment	1578				

[a] Calculated using dipole moments obtained from SCF wavefunctions. [b] Calculated from the $\nu_1 + \nu_3$ combination band observed at 2003 cm^{-1}. [c] Calculated from the $\nu_1 + \nu_3$ combination band observed at 1322 cm^{-1}. [d] HXeO out-of-plane bend. [e] Xe–OH stretch.

corresponds to the lowest energy path for dissociation of the molecules, is predicted to decrease by about 100 cm^{-1} from its harmonic value.

The anharmonic vibrational calculations are based on the ab initio calculated points on the potential energy surface, which allows us to estimate the wavenumbers of the combinations overtones. For example, an experimentally observed band at 2003 cm^{-1} belongs to HXeH, but no conclusive assignments for this mode could be given. The anharmonic MP2 calculations predict the combination band of the symmetric and antisymmetric stretchings to have significant intensity, and we can assign the 2003 cm^{-1} band accordingly. This gives us an indirect measure of the IR-inactive symmetric stretch, which should be at ca. 840 cm^{-1}. The derived wavenumber is much lower than predicted by any computational methods using harmonic approach to calculate the vibrational frequencies.

The X–H stretching motion is an essential part of the vibrational calculation of the HXY molecules. For more strongly bound HXY molecules the MP2 vibrational calculations become better but HXeH (as well as HXeSH) represents a borderline case and require more sophisticated computational approaches. In the course of our work, we have found that even the moderate MP2 calculations give reasonable qualitative results not only for the structures, charge separation and vibrational frequencies but also for the large intensities of the X–H stretching absorptions. The calculated intensities for the Xe–H stretch in various molecules are shown also in Table 2. For the strongly bound molecules like HXeCl and HXeBr, the MP2 calculations are good enough to reproduce the correct molecular properties and PES characteristics. Even though the computational vibrational frequencies are generally overestimated the systematic trend among the pre-
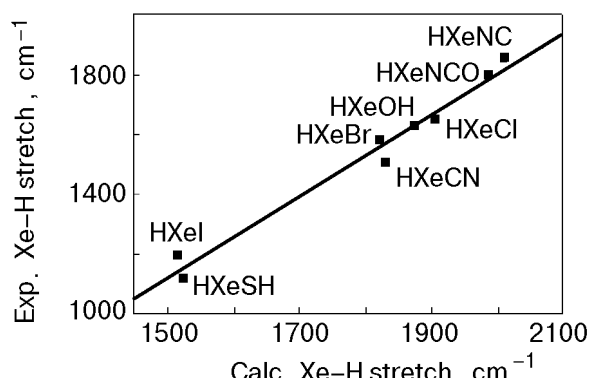
Fig. 2. Comparison of calculated (MP2) and experimental Xe–H stretching values for HXY molecules.

sent HXY molecules is correctly predicted. When a HXY molecule is strongly bound, the Xe–H bond distance is shorter and this is reflected as a blueshift of the X–H stretching vibration. This is in accord with the experimental Xe–H wavenumbers which shift to higher values from the weakest bound HXeSH to the strongest bound HXeNC, as shown in Fig. 2, where the experimentally observed Xe–H stretching wavenumbers are plotted against the calculated harmonic values. For comparison, the XeH$^+$ vibrational frequency in the gas phase has been reported at 2270 cm^{-1} [78].

Experimental results

Formation of HKrY *and* HXeY *molecules.* The starting point for solid-state synthesis of the HXY molecules is to choose a hydrogen-containing precursor like H_2O, H_2S, hydrogen halides, HNCO, etc. The precursor molecule (HY) is diluted with excess of krypton or xenon, and the mixture is trapped on a cold surface of an IR transparent window. It is important that the precursor is as monomeric as possible, since precursor aggregation complicates the photochemistry, as shown, for example, in the case of hydrogen halides [86]. In order to promote the isolated precursor to a dissociative state, various light sources can be used. For hydrogen halides simple UV lamps are suitable since the dissociation energies of these molecules are around 4 eV [87]. Additionally in the preparation of HXY molecules, excimer lasers (248, 193, and 157 nm) and tunable (down to 225 nm) radiation of an optical parametric oscillator have been used. The main objective of the photodecomposition process is to separate the H and Y fragment of the HY precursor. The extent of the mobility of the fragments during the primary photolysis, especially of the hot H atoms, will be addressed below.

Upon photolysis, neutral fragments H and Y are localized in a rare gas matrix. For example, in the cases of HI and HBr the presence of I and Br atoms is clearly evidenced by their spin-orbit ($^2P_{1/2} \leftarrow {}^2P_{3/2}$) absorptions at ca. 7600 and 3600 cm^{-1}, respectively [61]. Both the H atoms and Y fragments are stable below the mobilization temperature of hydrogen atoms (30–50 K). In very dilute matrices (M/A ratio > 1000), it is possible to convert a major part of the precursor to H atoms and neutral Y fragments. In more concentrated matrices, other processes like clusterization and photoinduced reactions of hydrogen atoms produce more complicated products as well as hydrogen molecules [61,88]. The second step in the solid-state synthesis of HXY molecules is annealing of the photolyzed matrix to the point where the H atoms start to diffuse. Several separate experiments have shown that the diffusion occurs at ca. 30 and 40 K in solid Kr and Xe [59,88–93]. The diffusing H atoms find eventually a rare gas atom which has a fragment Y as a near neighbor, and the three fragments H, Y, and X react forming the HXY molecule. Reaction of two hydrogen atoms with a Xe atom between them produce HXeH. In the case of krypton, this last reaction has not been observed to occur, and also computationally HKrH molecule is unstable. Most importantly, in solid Xe the HXeY and HXeH molecules seem to be the major trapping sites for H atoms and Y fragments in solid rare gases after mobilization of hydrogen atoms [65].

A valuable observation was made concerning the formation of the HXeNCO molecule in HNCO photolysis in solid Xe [68]. The rare gas molecule was observed to form not only in the annealing but also directly in the photolysis of HNCO. The kinetics of HXeNCO was followed during 193 nm photolysis, and the HXeNCO molecule rises rapidly, reaches a maximum and decreases eventually completely due to its own photodecomposition. The experiment was performed photolyzing HNCO using different wavelengths (225, 240, 250, 266 nm) but the formation of HXeNCO was observed to occur only at 193 nm irradiation. The maximum concentration of HXeNCO produced during photolysis was estimated to be about 0.4% from the initial concentration of the precursor HNCO. There are different alternatives for the mechanism of formation of HXeNCO: HXeNCO can be formed directly from HNCO/Xe in a photoisomerization process, or it can be formed from a hydrogen atom loosing its kinetic energy in the immediate vicinity of the NCO fragment. Nevertheless, once formed the subsequent

photodecomposition of HXeNCO provides much more kinetic energy to the H atom than the direct dissociation of the HNCO precursor at the same irradiation wavelength. Finally, it should be noted that HXeNCO can be decomposed by 405 nm irradiation and it produces HNCO and H + NCO with a branching ratio of 70%/30% [68].

In general, the HXY molecules are easily detected by IR spectroscopy due to the extremely intensive X–H stretching absorptions [56–60,62–64,68], and the position of the stretching band is very characteristic for each Y. In addition to the Xe–H absorption bands, other bands like combinations, overtones and fundamental bands characteristic of the Y-residue in the HXY molecules have been observed, and they are collected in Tables 2 and 3 including also frequencies for the deuterated species. A striking example of the sensitivity of the ν(Xe–H) absorption on the properties of the Y fragment is found by comparing the two isomers of HXeCN. The lowest energy isomer HXeCN the ν(Xe–H) absorption is at 1624 cm^{-1} and it shifts by + 227 cm^{-1} to 1851 cm^{-1} for the higher energy species HXeNC [59]. In fact, this also measures the anisotropy of the CN fragment.

Several vibrational overtones and combinations have been reported for the HXY molecules (see Table 2). For HXeI and HXeBr both the bending and the Xe–H stretching overtones show measurable intensities arising from anharmonic effects. The most striking effect is the enhanced intensity of the bending overtones compared with the fundamental bands for HXeBr and HXeI. For HXeCl, the bending overtone is predicted by anharmonic MP2 calculations to be of small intensity, and indeed, this vibration has not been observed experimentally. For the Xe–H stretching vibrations of HXeBr and HXeI, the first overtones are computationally rather weak compared with the fundamental modes but they are still intensive enough to be experimentally observed.
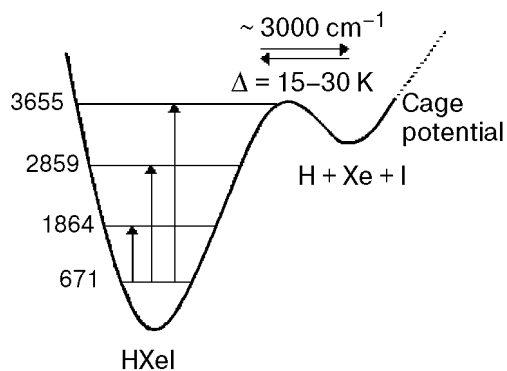

Fig. 3. Photodissociation upon IR irradiation and recombination upon annealing of HXeI.

The observed IR absorptions (in cm^{-1}) of different HXeY and HKrY compounds

Compound	ν [X–H(D)]	δ [H–X–Y]	ν [X–Y]	ν [Y]
HXeCl	1648			
DXeCl	1198			
HXeBr	1504	489		
DXeBr	1100			
HXeI	1193	450	129[a]	
DXeI	893			
HXeCN	1624			
DXeCN	1178			
HXeNC	1851			2044 (νCN)
DXeNC	1339			
HXeNCO	1788			2148 (ν_{as}NCO)
DXeNCO	1299			2145 (ν_{as}NCO)
HXeOH	1578			
HXeOD	1572			
DXeOH	1149			
DXeOD	1141			
HXeSH(D)	1119			
DXeSH(D)	833			
HXeH	1166, 1181 (ν_{as}) 840 (ν_{sym})[b]	701		
HXeD	1093 (νXe–H) 753 (νXe–D)	621		
DXeD	846, 856	514		
HKrCl	1476	544		
DKrCl	1106			
HKrCN	1497	618		
DKrCN	1109			

a) Calculated from the difference between the $\nu_1 + \nu_3$ combination band (1322 cm^{-1}) and the antisymmetric stretch (ν_3, 1193 cm^{-1}). b) Calculated from the difference between the $\nu_1 + \nu_3$ combination band (2003 cm^{-1}) and the antisymmetric stretch (ν_3, 1166 cm^{-1}).

The overtones of HXeI have played an important role in resolving the mechanism of formation of the HXY molecules [58]. The ν(Xe–H) frequency of HXeI is at 1193 cm^{-1}, 2ν(Xe–H) is at 2190 cm^{-1}, and around energies 3ν(Xe–H) close to 3000 cm^{-1} the molecule decomposes [58]. This is schematically shown in Fig. 3. The HXeI infrared photodissoci-

ation experiment yields an absorption profile for the $3\nu(Xe-H)$ transition with an onset at 2950 cm^{-1}, which could be considered as an approximate value for the D_0 dissociation energy of HXeI. After the IR decomposition the molecular form can be restored by annealing at temperatures considerably below those needed for the global mobilization of H atoms in solid xenon. Therefore, the $3\nu(Xe-H)$ excitation of HXeI produces atoms in a close contact with each other and HXeI can be recovered by slight warming or even at the lowest temperatures by tunneling as pictured in Fig. 3. The increase of the spin-orbit absorption of iodine atoms at ca. 7600 cm^{-1} correlated with the infrared induced decrease of HXeI and vice versa [58]. The low energy of the infrared photons is not sufficient to produce ionic centers in the matrix indicates that the HXY molecules correlate with the neutral atom asymptote. Additional evidence for formation of HXY from neutral atoms is available from Feldman and coworkers [91,92]. These authors combined infrared and ESR-spectroscopic methods to study electron-irradiated xenon matrices containing various hydrocarbons, and they found that the decrease of hydrogen atoms correlated with the growth of HXeH. Adding electron scavengers which enhance ion formation decreased the yield of HXeH [91,92].

We can also estimate the anharmonicity of the $\nu(Xe-H)$ strecth from the experiments and the derived anharmonicity constant $(\omega_e x_e)$ is about 100 cm^{-1} in solid Xe [94]. This value has been used to calculate the energy levels of $\nu(Xe-H)$ in HXeI and they are marked accordingly in Fig. 3. The experimentally derived barrier height for the recombination of the neutral fragments to form HXeI is ca. 700 cm^{-1} [58].

As mentioned above, one of the weakest bound molecules HXeI dissociates already at $3\nu(Xe-H)$ excitation. Besides this, the electronically excited states lead to decomposition of the HXY molecules. All HXY molecules decompose with visible or UV light, and the decomposition onsets vary from near IR to 350 nm. HXeH was found to be the most photostable member of this family, and it is rather long-lived under 400 nm irradiation. The electronic states involved in the photodecomposition of the HXY molecules are not known yet but there exist a trend in the VIS-UV-stability of these molecules. For example, the onset of photodecomposition of the halogenated xenon hydrides is the following: HXeI dissociates at wavelengths below ~ 700 nm, HXeBr below ~ 450 nm and the most stable of this series, HXeCl, requires wavelengths below ~ 350 nm.

Production of H *atoms in photolysis of small hydrides in solid* Xe. Experimental preparation of the HXY hydrides is closely connected with the dynamics of H atoms in rare-gas solids, both during photolysis and annealing. General description of these processes can be found in a recent review by Apkarian and Schwentner [54], and we discuss below only some aspects of solid-state photolysis related to the present consideration. A number of experiments with HXeY compounds allow us to estimate the absolute amount of H atoms generated under UV photolysis of an HY precursor in solid Xe. Especially, this consideration concerns light-induced travel distances of «hot» H atoms after photolysis and their losses via the two most evident reactions: $H + H \rightarrow H_2$ and $H + HY \rightarrow H_2 + Y$. This approach allows us to distinguish the local and global primary photolysis events.

The UV photolysis of HI, HCN and HNCO in Xe was studied, and concentrations of I atoms, CN or NCO radicals were measured by IR absorption spectroscopy [58,59,68]. It was found that annealing of the photolyzed matrices at 40–50 K decreases the concentration of I atoms, CN or NCO radicals typically by about 40%, and this decrease was attributed to the formation of HXeI, HXeCN and HXeNCO molecules. Furthermore, HXeH molecules were formed in annealing consuming some part of the photo-generated H atoms. The results clearly indicate that the amount of H atoms after photolysis is comparable with the amount of the other dissociated part (I, CN, or NCO), and also with the amount of the photolyzed precursors. It follows that loss channels due to extensive mobility of H atoms do not play a major role during photolysis of HY precursors in monomeric matrices.

Ternary HI/CO/Xe matrix mixtures were prepared in order to estimate the lower limit of the H atom concentration produced in photolysis by monitoring the decrease of CO during annealing due to the reaction $H + CO \rightarrow HCO$ [69]. A HI/CO/Xe = 1/2/2000 matrix was extensively photolyzed at 310 nm. Upon annealing, the amount of formed HCO corresponded to ~ 15% of photolyzed HI, and HXeI and HXeH were formed with an efficiency similar to the case of CO-free matrices. During the photolysis, HCO appeared but its amount remained an order of magnitude smaller than the amount measured after annealing. Thus, the proportion of H atoms consumed to HCO during the photolysis is about 1% despite the twice-higher CO concentration compared to that of HI. This observation indicates the low probability for the distant reaction of the hot H atom with CO
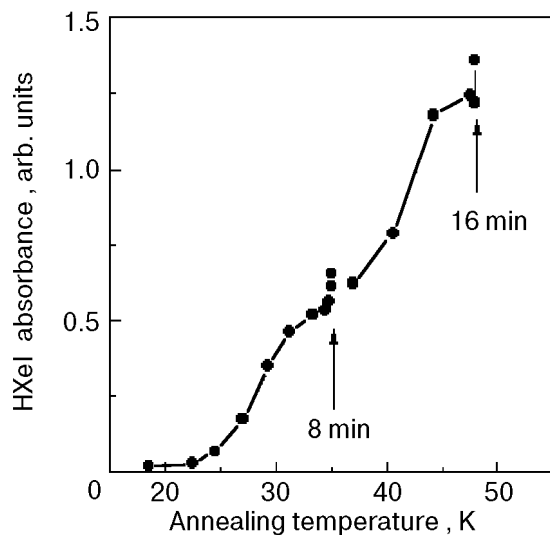
Fig. 4. The formation of HXeI molecules in annealing. The HI/Xe (1/2000) matrix was photolyzed at 310 nm. The annealing was performed with the 2 K/min rate. At temperatures 35 and 48 K warming up was stopped for about 8 and 16 min in order to check the saturation of the reaction.

or/and short-distance travel of H atoms. It is plausible that a similar inefficiency is also applicable to losses via the reactions $H + H \rightarrow H_2$ and $H + HY \rightarrow H_2 + Y$.

Thus, it can be concluded that losses of hot H atoms due to extensive light-induced travel in a low-temperature Xe lattice are quite minor. Moreover, the losses of H atoms during annealing seem to be essentially due to the formation of Xe-containing molecules. On the other hand, additional losses are evidenced by the gradual decrease of HXeI in multiple cycles of annealing and selective light-induced decomposition of HXeI [69], and formation of H_2 molecules is the most probable process. In this respect, the diffusion-limited reactions of H atoms with HXeH and HXeY molecules should be taken into account.

As mentioned earlier, the losses of H atoms during UV photolysis should be connected with its light-induced travel distance. The experiments with rare-gas containing molecules at various precursor concentrations support only very limited light-induced travel distances under UV photolysis in solid Xe. In this respect, the efficient generation of HXeI in low-temperature annealing (~ 30 K) of photolyzed HI/Xe matrices is an important observation [69]. The increase of HXeI during annealing is presented in Fig. 4. Two stages of annealing producing HXeI can approximately be distinguished around 28 and 40 K, and they should be qualitatively connected with local and global mobility of H atoms. Indeed, it is well established that the

global mobility of H atoms in solid Xe starts at temperatures above 38 K [92,93]. On the basis of the efficient low-temperature formation of HXeI, we have suggested a quite local distribution of H atoms in the primary photolysis of HI in solid Xe [69]. In this model, the locally trapped H atoms can form HXeI via reacting with the parent I atom in the low-temperature annealing similarly as discussed above for the IR decomposition of HXeI. Furthermore, the local distribution of H atoms generated in photolysis agrees with the absence of major losses of H atoms during primary photolysis. This conclusion of minor losses of H atoms *during photolysis* should be distinguished from the diffusion-controlled processes *during annealing* when H atoms move globally and may quite efficiently form H_2 molecules as mentioned earlier.

The experimental model of local photolysis agrees completely with the molecular dynamics simulations of 273 nm photolysis of HI in solid Xe [95,96]. These computations indicate that the photolysis of HI is a rather local process and the obtained trajectories lead to trapping of the H atom in the nearest interstitial sites. Eloranta et al. employed another approach in simulating the distribution of H atoms under photolysis in different rare-gas matrices [97]. In their study, an H atom was placed into a substitutional site of a perfect fcc lattice and provided with 2.5 eV of kinetic energy, and most of the resulting trapping position in solid Xe corresponded to the nearest interstitial site.

Experiments with HXeI molecules suggest the existence of hidden secondary processes during photolysis [69]. The proportion of HXeI forming in low-temperature annealing (< 38 K) becomes smaller for longer irradiation times. Most importantly, this proportion decreases further with irradiation time even after *complete* decomposition of HI, approaching zero for very long irradiation. The HXeH/HXeI ratio measured after annealing at 48 K increases with irradiation time, and it is influenced by the irradiation time after the complete decomposition of HI as well: it increases in the prolonged photolysis. On the basis of these observations, it was concluded that H atoms could be driven from the parent cage not only in the preliminary decomposition of HI but also in some secondary processes involving other species. The first hidden process was suggested to be neutralization of Xe_2H^+ that provides kinetic energy for the H atom when the Xe atoms relax quickly from the perturbed (bound) configuration to their lattice positions. The mobile electrons providing the neutralization are photodetached from the Y^- fragments.

The other proposed hidden process involves the HXeI potential surface: if an escaping H atom forms the HXeI intermediate, it can gain more kinetic energy in photodecomposition of the HXeI molecules. In consonance with the latter hypothesis, HXeNCO was found to form directly in photolysis of HNCO in solid Xe as described earlier [68]. In the case of HI, no detectable amount of HXeI is observed in the photolysis of HI, which is most probably due to a very effective photodissociation of HXeI. Up to now, the computer simulations on photolysis of HI in solid Xe do not include the molecular HXeI potential, and this neglect might be a severe oversimplification of the system suggesting theoretical reinvestigation of the process.

Some controversial conclusions on the dynamics of small hydrides in rare-gas solids can be found in literature. LaBrake et al. suggested a migration distance of ~ 10 nm for H atoms upon 193 nm photolysis of HBr in a Xe matrix, extensive losses of H atoms via the H + HBr $\rightarrow$ H$_2$ + Br reaction, and a very small amount of H atoms generated in the photolysis [88]. The conclusions derived in Ref. 88 are based on the deviation of the LIF (laser-induced fluorescence) kinetics of photodissociative fragments from the simplest one-exponential form. Some support for such extensive losses was obtained by Eloranta et al. who reported extremely low amounts of H atoms in UV photolysis of HBr and HCl in a Xe matrix based on the very weak EPR signals from H atoms [97]. In a more recent paper of their laboratory [98], a possibility has been presented that the signal from H atoms trapped only in lattice substitutional sites was measured in Ref. 97.

The origin for the disagreement between the LIF and IR absorption estimates of the photoproduct concentrations in rare-gas matrices can be explained by taking into account the evolution of matrix optical properties during photolysis. The problem with quantitative analysis of photolysis kinetics by using LIF measurements was explicitly demonstrated experimentally. For instance, in the 193-nm photolysis of HCN/Kr matrices, the 775-nm emission of CN clearly saturates faster than its IR absorption does (Fig. 5) and this saturation was explained by self-limitation of the photolysis [63]. Other related examples can be found elsewhere [67]. The observed disproportion evidently breaks the assumption of proportionality between the LIF signal and the product concentration used in Ref. 88, casting strong doubts about the numerical estimates of travel distance and losses of H atom during HBr photolysis in Xe.
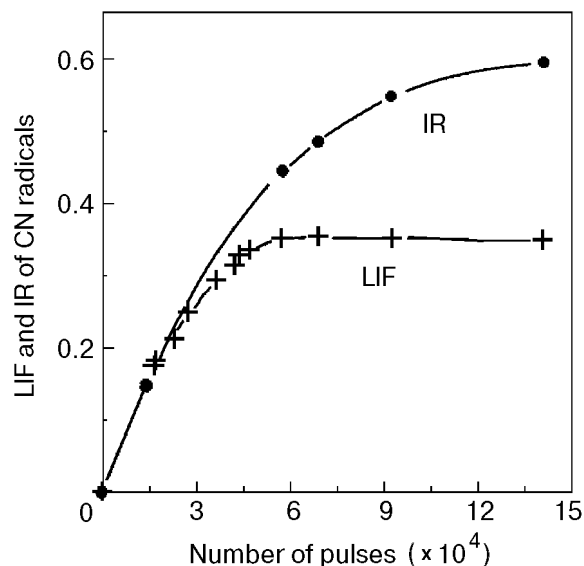

Fig. 5. The LIF and IR absorption kinetics of CN during 193 nm photolysis of a HCN/Kr matrix at 7.5 K. The last data point corresponds to decomposition of 65% of HCN.

In order to describe LIF kinetics properly, a number of factors should be considered, being extremely difficult to do in practice. First, rare-gas solids can often not be regarded as optically thin, and the depletion of the excitation field during its penetration into the matrix layer plays an important role in quantitative kinetics studies [63,67,99–101]. If a sample contains a sufficient number of precursor molecules, photogenerated new species can essentially absorb the photolysis radiation and hence decrease strongly the photolysis efficiency for deeper matrix layers. Hence the in situ-detected LIF signal of the photogenerated species saturates faster than their averaged concentration does [63]. This effect was also qualitatively discussed by Gödderz et al. [102].

The second factor strongly influencing LIF kinetics is introduced by photogenerated species that are capable of absorbing the detected emission. This process can change the detected LIF spectra from different matrix depths strongly thereby introducing an additional error between the LIF and true kinetics. One example of rising absorbers is provided by a charge-transfer mechanism known for species like oxygen, iodine, etc. in rare-gas solids [99,100,103]. The extraordinary disappearance of one emission band in the NO progression generated in the 193-nm photolysis of HNCO/Xe matrices was explained by considering a charge-transfer absorption [67].

Finally, Rayleigh scattering enhances the two above-mentioned mechanisms because it increases the path length of radiation in the sample and limits

penetration of the radiation into the deeper matrix layers even if the matrix absorption is rather weak. Even alone, Rayleigh scattering destroys the ideal one-exponential photolysis kinetics for concentration due to spatial redistribution of radiation intensity [63].

Intrinsic properties. Until recently, the HXY molecules have been prepared in solid rare gases, mainly Kr and Xe. Since the molecules are strongly polar there arises the question of their intrinsic stability and of the stabilization effect of the polarizable hosts. To address this question of intrinsic stability, photolysis of HBr and HCl in Xe-doped neon matrices was performed [104]. Quite surprisingly, even at very high dilution mobilization of H atoms in Ne at ~ 9–10 K resulted in new absorptions at wavenumbers similar to the ν(Xe–H) of HXeBr and HXeCl in pure Xe matrices. These absorptions showed proper deuteration shifts for HXeBr and HXeCl, and the species responsible could be photodecomposed similarly to HXeBr and HXeCl in Xe. Based on these facts the forming molecules were identified as HXeBr and HXeCl in a Ne surrounding. This result shows experimentally the intrinsic stability of the HXY species supporting the computational results, and suggest for their existence also in the gas phase. The ν(Xe–H) wavenumbers of HXeCl and HXeBr in solid Ne are shifted about 50 cm^{-1} downwards from the values reported in Xe [56]. This shift can be considered to measure the stabilization effect of the solid Xe environment.

Conclusions

Solid state photochemical production of several Kr and Xe hydrides is described, and the IR spectra of these molecules are given. For aiding the experimental interpretation, extensive ab initio calculations were performed. Computationally, the formation of these hydrides decreases, for example, the Rg–H distance by more than a factor of two from its van der Waals value.

These HKrY and HXeY molecules possess both covalent and ionic contributions in the bonding, and their dipole moments are quite large. The extensive charge-transfer nature of these molecules is evidenced also by the strong Rg–H stretching vibrations both computationally and experimentally. These hydrides are produced in low temperature matrices by photodissociation of a hydrogen-containing precursor and thermal mobilization of photodetached hydrogen atom. The estimated dissociation energies vary from 0.4 to 1.4 eV, and warrant observation of these molecules also in the gas phase.

The photolysis of small hydrides in solid Xe seems to be a quite local process, and losses of H atoms play a minor role. The controversial estimates of the light-induced travel distances can originate from an improper treatment of LIF data. The effects of matrix optics become more important for shorter photolysis/LIF wavelengths due to Rayleigh scattering, and in particular they might be deeply problematic in vacuum UV experiments. As a qualitative conclusion of practical importance for matrix-isolation studies, matrix optics should be taken into account while extracting numerical dissociation parameters from LIF kinetics. In fact, FTIR measurements provide more reliable data for such a quantitative analysis.

1. L. Pauling, *J. Am. Chem. Soc.* **55**, 1895 (1933).
2. N. Bartlett, *Proc. Chem. Soc.* **218** (1962).
3. F. O. Sladky, P. A. Bulliner, and N. Bartlett, *J. Chem. Soc.* **A2179** (1969).
4. R. Hoppe, W. Dähne, H. Mattauch, and K. H. Rödder, *Angew. Chem.* **74**, 903 (1962).
5. H. H. Claassen, H. Selig, and J. G. Malm, *J. Am. Chem. Soc.* **84**, 3593 (1962).
6. J. R. Morten and W. E. Falconer, *J. Chem. Phys.* **39**, 427 (1963).
7. E. Tommila, *Suomen Kemistilehti* **A36**, 209 (1963).
8. J. G. Malm, H. Selig, J. Jortner, and S. A. Rice, *Chem. Rev.* **65**, 199 (1965).
9. F. O. Sladky, P. A. Bulliner, N. Bartlett, B. G. DeBoer, and A. Zankin, *Chem. Commun.* 1048 (1968).
10. V. M. McRae, R. D. Peacock, and D. R. Russell, *Chem. Commun.* 62 (1969).
11. J. H. Holloway and J. G. Knowles, *J. Chem. Soc.* A756 (1969).
12. N. Bartlett, M. Gennis, D. D. Gibler, B. K. Morrell, and A. Zalkin, *Inorg. Chem.* **12**, 1717 (1973).
13. D. E. McKee, C. J. Adams, and N. Bartlett, *Inorg. Chem.* **12**, 1722 (1973).
14. N. Bartlett and F. O. Sladky, *Comprehensive Inorganic Chemistry*, Pergamon Press, New York (1973), vol 3, p. 213.
15. K. Seppelt and D. Lentz, *Prog. Inorg. Chem.* **29**, 167 (1982).
16. J. H. Holloway, *J. Fluor. Chem.* **33**, 149 (1986).
17. C. A. Coulson, *J. Chem. Soc.* 1442 (1964).
18. R. D. LeBlond and D. D. DesMarteau, *J. Chem. Soc. Chem. Commun.* 555 (1974).
19. D. D. DesMarteau, *J. Am. Chem. Soc.* **100**, 6270 (1978).
20. D. D. DesMarteau, R. D. LeBlond, S. F. Hossain, and D. Nothe, *J. Am. Chem. Soc.* **103**, 7734 (1981).
21. A. A. A. Emara and G. J. Schrobilgen, *J. Chem. Soc. Chem. Commun.* 1644 (1987).
22. A. A. A. Emara and G. J. Schrobilgen, *J. Chem. Soc. Chem. Commun.* 257 (1988).
23. G. J. Schrobilgen, *J. Chem. Soc. Chem. Commun.* 1506 (1988).
24. J. Foropopoulos, Jr. and D. D. DesMarteau, *J. Am. Chem. Soc.* **104**, 4260 (1982).
25. J. F. Sawyer, G. J. Schrobilgen, and S. J. Sutherland, *Inorg. Chem.* **21**, 4064 (1982).
26. G. A. Schumacher and G. J. Schrobilgen, *Inorg. Chem.* **22**, 2178 (1983).

27. R. Faggiani, D. K. Kennepohl, C. J. L. Lock, and G. J. Schrobilgen, *Inorg. Chem.* **25**, 563 (1986).

28. M. Wechsberg, P. A. Bulliner, F. O. Sladky, R. Mews, and N. Bartlett, *Inorg. Chem.* **11**, 3063 (1972).

29. L. J. Turbini, R. E. Aikman, and R. J. Lagow, *J. Am. Chem. Soc.* **101**, 5833 (1979).

30. D. Naumann and W. Tyrra, *J. Chem. Soc. Chem. Commun.* 47 (1989).

31. V. V. Zhdankin, P. J. Stang, and N. S. Zefirov, *J. Chem. Soc. Chem. Commun.* 578 (1992).

32. D. Naumann, W. Tyrra, R. Gnann, D. Pfolk, T. Gilles, and K. F. Tebbe, *Z. Anorg. Allg. Chem.* **623**, 1821 (1997).

33. H. J. Frohn, N. LeBlond, K. Lutar, and B. Zemva, *Angew. Chem. Int. Ed.* **39**, 391 (2000).

34. J. H. Holloway and E. G. Hope, in: *Advances in Inorganic Chemistry*, Academic Press, London (1999), vol 46, p. 51.

35. J. J. Turner and G. C. Pimentel, *Science* **140**, 975 (1963).

36. D. R. MacKenzie, *Science* **141**, 1171 (1963).

37. W. F. Howard and L. Andrews, *J. Am. Chem. Soc.* **96**, 7864 (1974).

38. A. V. Grosse, A. D. Kirschenbaum, A. G. Streng, and L. V. Streng, *Science* **139**, 1047 (1963).

39. G. J. Schrobilgen, *J. Chem. Soc. Chem. Commun.* 863 (1988).

40. J. C. P. Sanders and G. J. Schrobilgen, *J. Chem. Soc. Chem. Commun.* 1576 (1989).

41. R. J. Gillespie and G. J. Schrobilgen, *Inorg. Chem.* **15**, 22 (1976).

42. G. J. Schrobilgen, *J. Chem. Soc. Chem. Commun.* 1506 (1988).

43. G. Frenking and D. Cremer, in: *Structure and Bonding, Noble Gas and High Temperature Chemistry*, M. J. Clarke et al. (ed.), Springer, Berlin (1990), p. 17.

44. G. J. Schrobilgen, in: *Synthetic Fluorine Chemistry*, G. A. Olah, R. D. Chambers, G. K. Surya Prakash (eds.) John Wiley and Sons, New York (1992).

45. I. Last and T. F. George, in: *Cluster Ions*, C. Y. Ng, T. Baer, and I. Powis (eds.), John Wiley and Sons, New York (1993) and References therein.

46. M. Beyer, E. V. Savchenko, G. Niedner-Schatteburg, and V. E. Bondybey, *J. Chem. Phys.* **110**, 11910 (1999).

47. P. Pyykkö, *Eur. J. Chem.* (2000) (in press).

48. E. Whittle, D. A. Dows, and G. C. Pimentel, *J. Chem. Phys.* **22**, 1943 (1954).

49. I. Norman and G. O. Porter, *Nature* **174**, 508 (1954).

50. H. Broida and J. R. Pellam, *Phys. Rev.* **95**, 845 (1954).

51. L. Y. Nelson and G. C. Pimentel, *Inorg. Chem.* **6**, 1758 (1967).

52. V. E. Bondybey, Doct. Thesis, *Univ. of California* (1971).

53. C. T. Goetschel and K. R. Loos, *J. Am Chem. Soc.* **94**, 3018 (1972).

54. V. A. Apkarian and N. Schwentner, *Chem. Rev.* **99**, 1481 (1999).

55. V. E. Bondybey, M. Räsänen, and A. Lammers, *Annu. Rep. Prog. Chem. Sect.* **C95**, 331 (1999).

56. M. Pettersson, J. Lundell, and M. Räsänen, *J. Chem. Phys.* **102**, 6423 (1995).

57. M. Pettersson, J. Lundell, and M. Räsänen, *J. Chem. Phys.* **103**, 205 (1995).

58. M. Pettersson, J. Nieminen, L. Khriachtchev, and M. Räsänen, *J. Chem. Phys.* **107**, 8423 (1997).

59. M. Pettersson, J. Lundell, L. Khriachtchev, and M. Räsänen, *J. Chem. Phys.* **109**, 618 (1998).

60. M. Pettersson, J. Lundell, L. Khriachtchev, E. Isoniemi, and M. Räsänen, *J. Am. Chem. Soc.* 7979 (1998).

61. M. Pettersson and J. Nieminen, *Chem. Phys. Lett.* **283**, 1 (1997).

62. M. Pettersson, *Doct. Thesis*, University of Helsinki (1998).

63. L. Khriachtchev, M. Pettersson, and M. Räsänen, *Chem. Phys. Lett.* **288**, 727 (1998).

64. M. Pettersson, L. Khriachtchev, J. Lundell, and M. Räsänen, *J. Am. Chem. Soc.* **121**, 11904 (1999).

65. M. Pettersson, J. Lundell, and M. Räsänen, *Eur. J. Inorg. Chem.* 729 (1999).

66. L. Khriachtchev, M. Pettersson, S. Pehkonen, E. Isoniemi, and M. Räsänen, *J. Chem. Phys.* **111**, 1650 (1999).

67. L. Khriachtchev, M. Pettersson, S. Jolkkonen, and M. Räsänen, *Chem. Phys. Lett.* **316**, 115 (2000).

68. M. Pettersson, L. Khriachtchev, J. Lundell, S. Jolkkonen, and M. Räsänen, *J. Phys. Chem.* **A104**, 3579 (2000).

69. M. Pettersson, L. Khriachtchev, J.-R. Roozeman, and M. Räsänen, *Chem. Phys. Lett.* **323**, 506 (2000).

70. N. Runeberg, M. Seth, and P. Pyykkö, *Chem. Phys. Lett.* **246**, 239 (1995).

71. N. Runeberg, *Doct. Thesis*, University of Helsinki (1996).

72. R. W. Bickes, Jr., B. Lantzsch, J. P. Toennies, and K. Walaschewski, *Farad. Discuss. Chem. Soc.* **55**, 167 (1973).

73. W. C. Lane, T. H. Edwards, J. R. Gillis, E. S. Bonomo, and F. J. Murcray, *J. Mol. Spectrosc.* **95**, 365 (1982).

74. J. Lundell, M. Pettersson, and M. Räsänen, *Computers and Chemistry* **24**, 325 (2000).

75. N. Franks and W. R. Lieb, *Nature* **367**, 607 (1994).

76. N. Bartlett, M. Wechsberg, G. R. Jones, and R. D. Burbank, *Inorg. Chem.* **11**, 1124 (1972).

77. I. Last and T. F. George, *J. Chem. Phys.* **89**, 3071 (1988).

78. J. W. C. Johns, *J. Mol. Spectrosc.* **106**, 124 (1984).

79. H. E. Warner, W. T. Connor, and R. C. Woods, *J. Chem. Phys.* **81**, 5413 (1984).

80. R. Klein and P. Rosmus, *Z. Naturforsch.* **39A**, 349 (1984).

81. K. A. Peterson, R. H. Petrmichl, R. L. McClain, and R. C. Woods, *J. Chem. Phys.* **95**, 2352 (1991).

82. S. A. Rogers, C. R. Brazier, and P. F. Bernath, *J. Chem. Phys.* **87**, 159 (1987).

83. S. Berski, B. Silvi, J. Lundell, S. Noury, and Z. Latajka, in: *Progress in Theoretical Chemistry and Physics*, C. Minot et al. (eds.), Kluwer, Amsterdam (2000) (in press).

84. M. Johansson, M. Hotokka, M. Pettersson, and M. Räsänen, *Chem. Phys.* **244**, 25 (1999).

85. J. Lundell, G. M. Chaban, and R. B. Gerber, *J. Phys. Chem.* **B104** (2000) (in press).

86. M. Lorenz, D. Kraus, M. Räsänen, and V. E. Bondybey, *J. Chem. Phys.* **112**, 3803 (2000).

87. H.Okabe, *Photochemistry of Small Molecules*, Wiley, New York (1978).

88. D. LaBrake, E. T. Ryan, and E. Weitz, *J. Chem. Phys.* **102**, 4112 (1995).

89. H. Muto, K. Nunome, and M. Iwasaki, *J. Phys. Chem.* **84**, 3402 (1980).

90. D. LaBrake and E. Weitz, *Chem. Phys. Lett.* **211**, 430 (1993).

91. V. I. Feldman and F. F. Sukhov, *Chem. Phys. Lett.* **255**, 425 (1996).

92. V. I. Feldman, F. F. Sukhov, and A. Yu. Orlov, *Chem. Phys. Lett.* **280**, 507 (1997).

93. J. Eberlein and M. Creutzburg, *J. Chem. Phys.* **106**, 2188 (1997) and References therein.

94. J. Lundell, M. Pettersson, L. Khriachtchev, M. Räsänen, G. M. Chaban, and R. B. Gerber, *Chem. Phys. Lett.* **322**, 389 (2000).

95. R. Alimi, R. B. Gerber, and V. A. Apkarian, *J. Chem. Phys.* **89**, 174 (1988).

96. R. Alimi and R. B. Gerber, *Chem. Phys. Lett.* **173**, 393 (1990).

97. J. Eloranta, K. Vaskonen, and H. Kunttu, *J. Chem. Phys.* **110**, 7917 (1999).

98. T. Kiljunen, J. Eloranta, and H. Kunttu, *J. Chem. Phys.* **110**, 11814 (1999).

99. M. E. Fajardo and V. A. Apkarian, *J. Chem. Phys.* **85**, 5660 (1986).

100. M. E. Fajardo and V. A. Apkarian, *J. Chem. Phys.* **89**, 4102 (1988).

101. J. R. Sheats, J. J. Diamond, and J. M. Smith, *J. Phys. Chem.* **92**, 4922 (1988).

102. K. H. Godderz, N. Schwentner, and M. Chergui, *J. Chem. Phys.* **105**, 451 (1996) and References therein.

103. W. G. Lawrence and V. A. Apkarian, *J. Chem. Phys.* **97**, 2229 (1992).

104. M.Lorenz, M. Räsänen, and V. E. Bondybey, *J. Phys. Chem.* **A104**, 3770 (2000).